Effects of E-BEAM Sterilization on Drug-Eluting Stents: Paclitaxel Degradation Elucidated by LC–MS–MS with Information-Dependent Acquisition

Yuri V. Il'ichev* and **Lori Alquier**
Cordis Corporation, Welsh and McKean Rds., Spring House, PA 19477

Abstract

Effects of sterilization by electron beam (E-BEAM) on paclitaxel (*1*) mixed with poly(DL-lactide-*co*-glycolide) (PLG) in reservoirs of COSTAR Stents are examined by using liquid chromatography-mass spectrometry (LC–MS–MS) techniques with information-dependent acquisition (IDA). Numerous degradation products of *1* are formed in a β-radiation dose-dependent manner to give plethora of low-level degradants. This behavior, together with multiple interferences from PLG-related compounds, creates considerable challenges for analysis of the drug/PLG mixtures. IDA methods with different survey scans are proven to be very efficient in elucidating degradation pathways and in identifying numerous products. Combined LC–MS–MS results from analysis of sterilized drug substance and stents indicate that water addition and oxidative processes together with the isomerization are largely responsible for degradation of *1* under E-BEAM sterilization conditions used.

Introduction

Paclitaxel (*1*) is a natural compound with a unique mechanism of cytotoxicity (1,2). This potent anticancer agent found applications in drug-eluting stents (3–5). Coronary stenting with local delivery of a therapeutic agent offers multiple advantages in comparison to other angioplasty procedures. Relatively high rates of repeat interventions seen for such procedures are mainly attributed to restenosis, the re-narrowing of a blood vessel after a successful coronary intervention. The use of *1* to prevent restenosis is mainly based on its anti-proliferative action (3–5). This, together with the lipophilic character of *1,* makes it a good candidate for localized delivery. The COSTAR Drug-eluting Stent (Conor Medsystems Inc.) employs *1* (Figure 1) as the drug and poly(DL-lactide-*co*-glycolide) (PLG) as a biodegradable polymeric matrix controlling the drug release (6–8). One of the essential requirements for a drug delivery platform is that it has to withstand sterilization. Understanding of mechanisms of drug degradation under sterilization conditions is, therefore, of primary importance for development of drug-eluting stents.

The paclitaxel molecule bears several ester groups (Figure 1) and, therefore, is expected to be susceptible to hydrolytic degradation (9,10). Baccatin III (*2*) and *N*-benzoyl-3-phenyl-*iso*-serine (*3*) may result from the degradation of (*1*). In addition, epimerization at the C7 atom and rearrangements involving the oxetane ring are among typical degradation mechanisms in solution (9–14). All the reactions mentioned above can be acid- or base-catalyzed. Electrochemical reduction of paclitaxel leads mainly to 10-deacetylpaclitaxel, which is also a common product of hydrolytic degradation (9).

No specific studies addressing *1* degradation mechanisms under electron-beam (E-BEAM) sterilization conditions could be found. However, a recent study of paclitaxel-eluting stents utilizing acrylate-based copolymer demonstrated no significant change in the drug elution profile upon exposure to 75 kGy of E-BEAM radiation (15). This dose was three times higher than the nominal dose used for medical device sterilization. Another

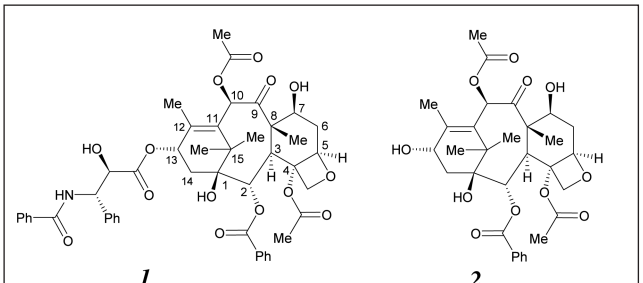

1
Formula: $C_{47}H_{51}NO_{14}$
Exact Mass: 853.33
$[M+Na]^+$ *m/z* 876.32

2
Formula: $C_{31}H_{38}O_{11}$
Exact Mass: 586.24
$[M+Na]^+$ *m/z* 609.23

3
Formula: $C_{16}H_{15}NO_4$
Exact Mass: 285.10
$[M+Na]^+$ *m/z* 308.09

4
Formula: $C_{47}H_{51}NO_{14}$
Exact Mass: 853.33
$[M+Na]^+$ *m/z* 876.32

Figure 1. Structural formula, exact masses, and mass-to-charge ratios for paclitaxel (*1*) and related compounds.

*Author to whom correspondence should be addressed: email iilitche@its.jnj.com

study (16) on the TAXUS Express Paclitaxel-eluting Stent showed no change in drug elution and impurity profiles for β–radiation dose up to 46 Gy. Under γ-irradiation conditions, ***1*** was found to be stable up to doses of 25 kGy (17). ***1*** has been reported to form ***4***, which is an isomer of ***1*** with the modified core structure, upon photoirradiation (18).

Preliminary studies of COSTAR Stents sterilized by E-BEAM revealed a large number of degradants that were formed at fairly low levels. This behavior, combined with the low drug dosage used, created serious challenges for analytical method development. The presence of the degradable polymer, PLG, imposed additional analytical requirements far beyond those commonly encountered in characterization and stress-testing of drug products (19).

This study was aimed at demonstrating how the QTRAP technology (20,21) could be utilized in the analysis of complex mixtures such as extracts of stressed COSTAR Stents. QTRAP refers to a commercial name of hybrid triple-quadrupole linear ion-trap mass spectrometers (MS), also known as QqQ_{LIT}, introduced by Applied Biosystems/MDS SCIEX. When combined with high-performance liquid chromatography, versatile scanning capabilities of these hybrid mass detectors have found numerous applications in drug discovery and metabolism, proteomics and lipidomics, screening for pollutants and toxicology-relevant compounds (22–31). In many cases, IDA-type methods were utilized to maximize the amount of information collected in a single chromatographic run and to facilitate data mining (26,28,30–34). IDA (Information Dependent Acquisition) is a data acquisition process in which the mass spectrometer actions can be varied from scan to scan based on data acquired in a previous scan.

Materials and Methods

Materials and samples

COSTAR Stents (non-sterile and sterilized by E-BEAM), paclitaxel-containing films of poly(DL-lactide-*co*-glycolide) (PLG) and photodegradant (***4***) were provided by Conor Medsystems (Menlo Park, CA). The PLG copolymer with a lactide-to-glycolide ratio of 85:15 was used. A 13-Taxane HPLC Mix Standard containing 10-deacetylbaccatin III, baccatin III, 10-deacetyl-7-xylosyltaxol B, taxinine M, 10-deacetyl-7-xylosyltaxol, 10-deacetyl-7-xylosyltaxol C, 10-deacetyltaxol, 7-xylosyltaxol, cephalomannine, 10-deacetyl-7-epitaxol, paclitaxel, taxol C, and 7-epi-taxol (~50 µg/mL of each taxane in methanol, 0.1% acetic acid) was obtained from Hauser Pharmaceutical Services. Paclitaxel (***1***, LC Laboratories), baccatin III (***2***, Bosche Scientific), and *N*-benzoyl-3-phenyl-*iso*-serine (***3***, Sigma-Aldrich) were used as received.

Samples were typically prepared by dissolving solids in acetonitrile. Three to five stents were combined and extracted with 1.0 mL of solvent. For paclitaxel-PLG films, samples for LC–MS–MS analysis were also prepared by a combined extraction/dissolution procedure. A piece of the polymer film was first extracted with a mixture of water, acetonitrile, and formic acid (FA) (62:38:0.1 wt.). The remaining solid was dried and dissolved in acetonitrile containing 0.1 wt% FA.

Sterilization

Stents and paclitaxel/PLG films were sterilized by E-BEAM irradiation to a dose of either 25 (1×) or 75 kGy (3×). For stress testing, stents were unpacked and exposed to ambient environmental conditions. Raw materials of ***1–3*** were also subjected to β-irradiation to three different doses: 25, 75, and 150 kGy. The irradiation was performed by using a 10 MeV electron beam accelerator (E-BEAM Services, Inc).

LC–MS–MS analysis

The LC–MS–MS setup consisted of an Agilent 1100 HPLC system (Santa Clara, CA) and an Applied Biosystems/MDS Sciex 4000 QTRAP mass spectrometer (Carlsbad, CA). Ionization was accomplished using a Turbo V source equipped with a TurboIonSpray (TIS) probe (Applied Biosystems). A Chromolith RP-18e column (Merck, Darmstadt, German. Dimensions: 4.6 × 100 mm, monolithic silica) was used. Column temperature was 35°C and the flow rate used was 1.5 mL/min. The flow was split with approximately 25% of the flow going to the ion source. The mobile phase solutions were prepared by instrument mixing of water (A) and acetonitrile (B). The two solvents were either used without any additives (Mobile phase A1/B1) or with 0.01% formic acid (FA, Fluka) added to both solvents (Mobile phase A2/B2). The following solvent program with linear gradients was utilized A/B: 98/2, 0–15 min; 98/2 to 65/35, 15–25 min; 65/35, 25–35 min; 65/35 to 54/46, 35–47 min; 54/46 to 2/98, 47–55 min; 2/98 to 98/2, 55–56 min; and 98/2, 56–65 min.

The IDA-type LC–MS–MS acquisition methods were used throughout the entire study. With the enhanced mass spectrum (EMS) scan as a survey scan, two dependent scans, enhanced res-

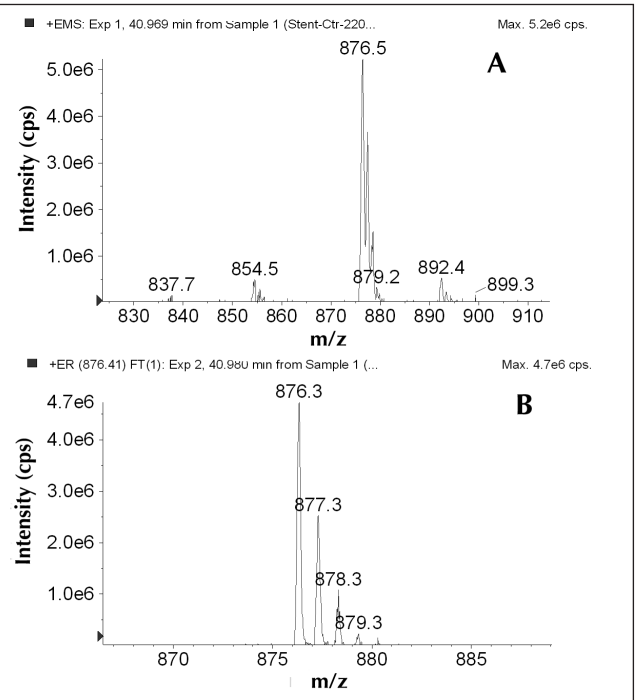

Figure 2. LC–MS–MS analysis of ***1*** in COSTAR Stent extracts. An enhanced mass spectrum (+EMS; A) recorded at 40.97 min and an enhanced resolution spectrum (+ER; B) recorded at 40.98 min are shown. Both spectra were acquired within the main chromatographic peak corresponding to ***1*** by using a non-sterile stent extract. Mobile phase: A1/B1.

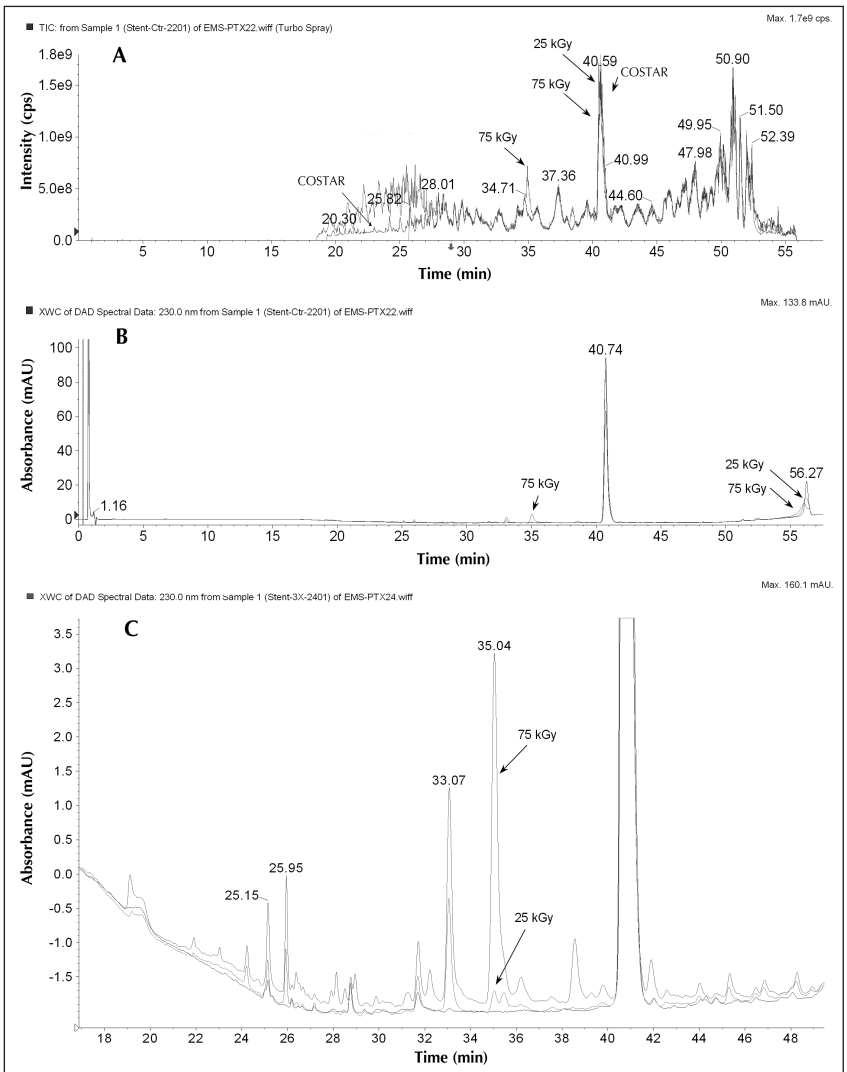

Figure 3. Total ion current chromatograms (A; TIC, sum of +EMS, +ER, +EPI) and extracted wavelength chromatograms (B and C; XWC of DAD, 230 nm) for non-sterile COSTAR Stent and stents sterilized by E-BEAM to a dose of 25 kGy and 75 kGy. Pane C presents a portion of the UV chromatogram showing major degradation products. Mobile Phase: A1/B1.

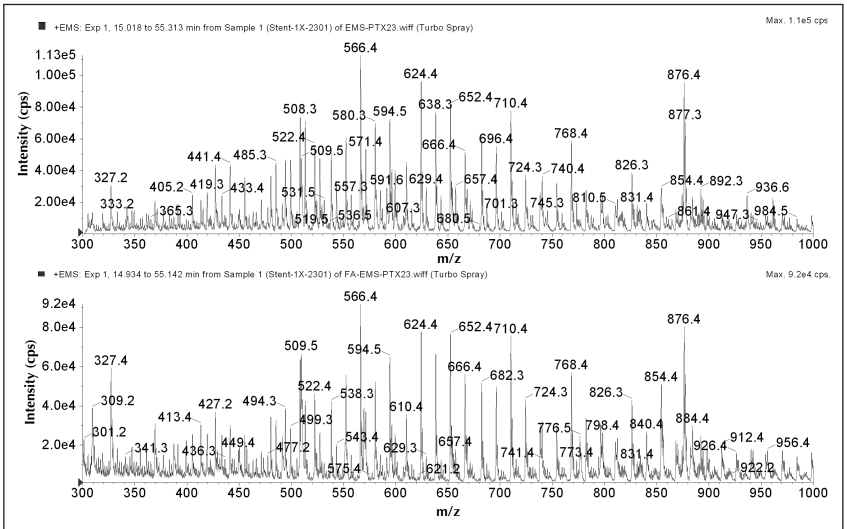

Figure 4. LC–MS–MS analysis of paclitaxel/PLG mixtures from stressed COSTAR Stents. Enhanced mass spectra (+EMS) recorded over the time range 15–55 min are presented. Mobile phase: A1/B1 (top), A2/B2 (bottom).

olution spectrum (ER) and enhanced product ion (EPI), were triggered when the intensity for the most abundant ion exceeded 200000 counts per second (cps). The IDA threshold was reduced to 500 cps for the methods with a Multiple Reaction Monitoring (MRM) survey scan. The scan rate for EMS and EPI was set at 4000 amu/s and ER utilized a scan rate of 250 amu/s. The following ion-source conditions were kept the same for all the scans: 670°C for the source temperature (TEM), 10, 25, and 30 psi for the curtain gas (CUR), nebulizing gas (GS1), and heating gas (GS2) pressures. The declustering potential (DP) was set at 100 V for all the scans except for the MRM scans, where a DP value of 80 V was selected. The EMS scans were performed over the range of 300–1000 amu, with the IonSpray voltage (IS) set at 1600 V, collision gas (CAD) at "Low" setting, and the collision energy (CE) at 5 eV. The IS value was reduced to 1300 V and the IDA threshold increased to 400000 cps when the FA-containing mobile phase was used (Mobile phase A2/B2). The setting for the MRM scans were as follows: IS = 4500 V, CAD = 6.0 (Medium), CE = 40 eV, collision cell exit potential (CXP) = 6.0 V. The dependent EPI acquisitions scanned the range of 140-1000 amu and used IS = 5500 V, CAD = 6.0, CE = 35 eV, an ion-trap fill time of 50 ms and the AutoFrag feature with CES = 10 eV (data acquired for CE = 25, 35, and 45 eV).

Results and Discussion

To characterize E-BEAM sterilization effects on ***1***, reversed-phase high-performance liquid chromatography (RP-HPLC) with ultraviolet and visible light absorption detection (UV) and mass spectrometric detection (MS) was used. Both RP-HPLC-UV and -MS data were acquired using spectral modes (i.e., both UV absorption and mass spectra were recorded for every time point during chromatographic separation). Mass spectral analysis of solutions of ***1*** in acetonitrile and its mixtures with water demonstrated that only weak MS signals could be observed with the negative polarity TIS (see Experimental Section) and that the deprotonated molecular ion, $[M–H]^-$ *m/z* 852.3, was very unstable for the MS conditions used. In contrast, positive-polarity TIS ionization produced very strong signals, mainly due to sodium adducts. LC–MS studies were further conducted using the positive polarity only. The IDA workflow for initial experiments was based on a full-scan MS acquisition. An enhanced mass spectrum (+EMS) scan followed by an enhanced resolution spectrum (+ER) were used to trigger an

enhanced product ion scan (+EPI) for the most abundant ion. The +EMS scan was used as a survey to detect all ions present; the +ER scan gave more accurate *m/z* values for the most abundant ion. The +EPI scan, which gave *m/z* values for product ions produced by collision-induced decomposition (CID) of the most abundant ion (precursor), provided structural information on the precursor ion and, therefore, served for more reliable identification.

The predominant ion observed for ***1*** under LC–MS conditions used was a sodium adduct, $[M+Na]^+$ *m/z* 876.32 (Figure 2). The protonated molecular ion ($[M+H]^+$ *m/z* 854.34) was also observed and the relative intensity of this ion signal increased by a factor of ~2.6 when formic acid (FA) was added to the mobile phase. Still, the sodium adduct signal remained the strongest for ***1*** and related compounds (see Figure 2). No evidence for an ammonium adduct of ***1*** ($[M+NH_4]^+$ *m/z* 871.37) was obtained from LC–MS analysis of drug substance solutions and stent extracts. The signal at the *m/z* close to 892 may be attributed to potassiated ***1*** ($[M+K]^+$ *m/z* 892.29) or a sodium adduct of its derivative with an additional oxygen atom ($[M+O+Na]^+$ *m/z* 892.32). The data presented below provides evidence for the presence of both species. Mass spectra of sodium and potassium adducts of ***1*** have been previously reported (35,36).

Figure 3 compares the total ion current (TIC) and extracted wavelength chromatograms (XWC) of acetonitrile extracts of non-sterile and E-BEAM sterilized stents. The TIC data correspond to MS signals summed over all the *m/z* values for the three scans. The UV chromatograms were dominated by two distinct peaks with retention times (RT) of 40.7 and 56.3 min. These two peaks were assigned to ***1*** and a high-molecular weight PLG, respectively, by using the HPLC-UV data for authentic materials, drug/PLG and PLG only films (compare Figure 3 with Figures S1 and S3 in Supplementary Information). Radiation dose-dependent degradation of ***1*** was evident from UV chromatograms that showed multiple individual peaks of low intensity (see Figure 3C). The UV data also indicated that the PLG peak (~56.3 min) strongly changed upon sterilization. For PLG, the predominant effect of ionizing radiation has been reported to be chain scission leading to depolymerization (37–39).

In contrast to the UV profiles, the mass chromatograms of stressed stent extracts showed numerous peaks fully covering the entire time range from 15 to 56 min. Figure 4 presents average mass spectra recorded over the time range 15–55 min. The addition of FA to the mobile phase resulted only in minor changes in the MS spectrum, which showed a distinct pattern with multiple series of peaks separated by 14 u. Similar MS spectra could be observed for solutions containing various PLG copolymers (data not shown). The vast majority of the peaks

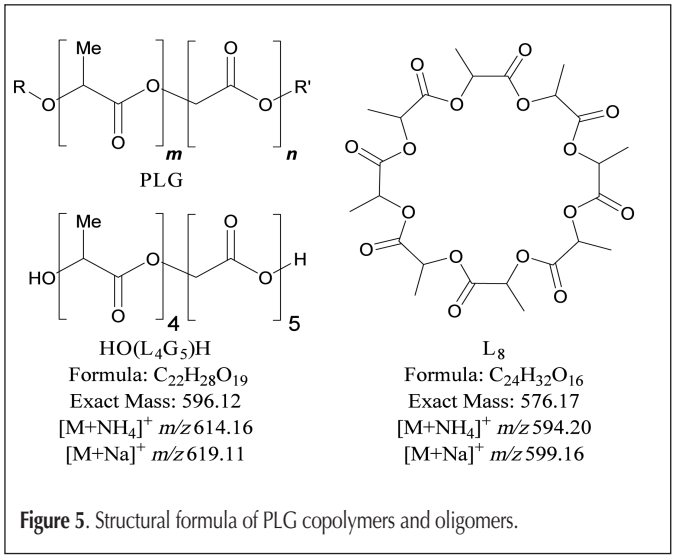

Figure 5. Structural formula of PLG copolymers and oligomers.

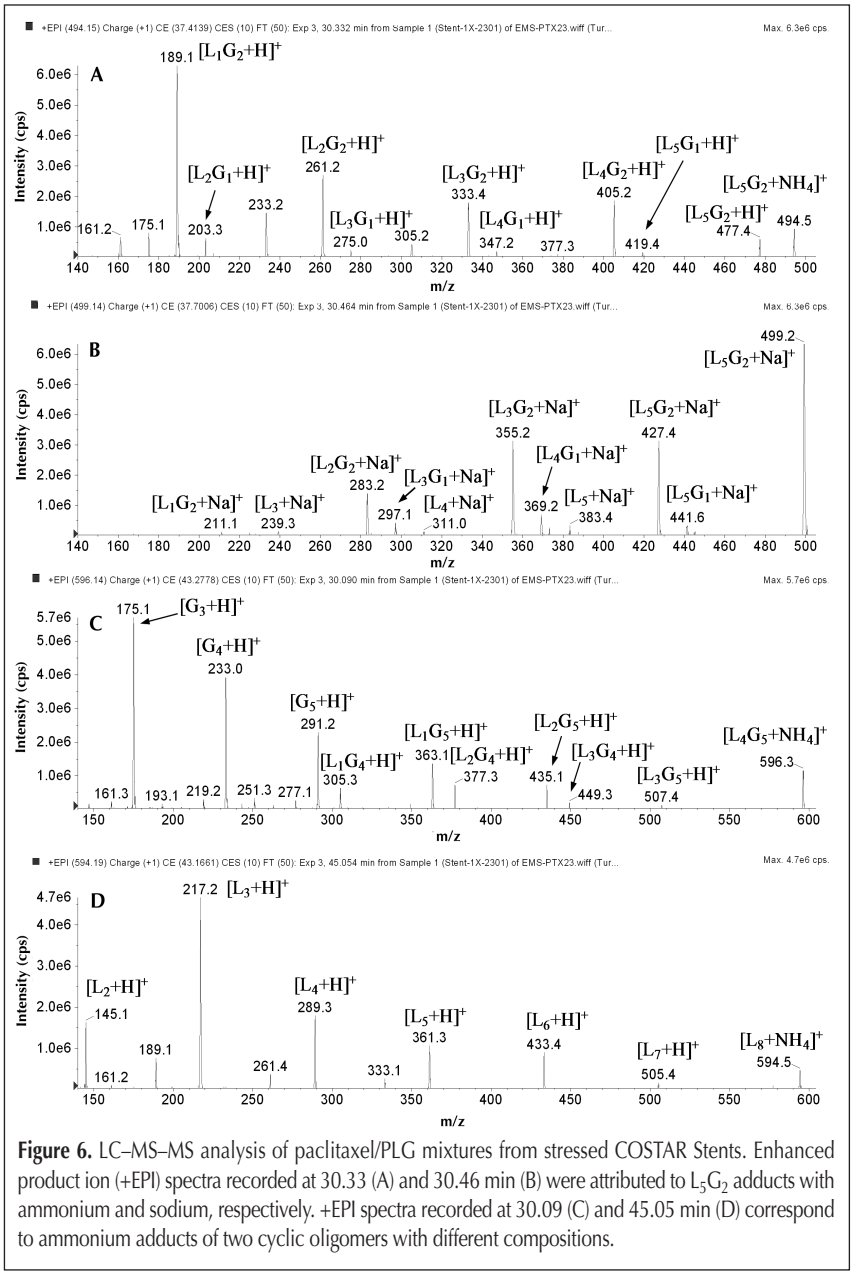

Figure 6. LC–MS–MS analysis of paclitaxel/PLG mixtures from stressed COSTAR Stents. Enhanced product ion (+EPI) spectra recorded at 30.33 (A) and 30.46 min (B) were attributed to L_5G_2 adducts with ammonium and sodium, respectively. +EPI spectra recorded at 30.09 (C) and 45.05 min (D) correspond to ammonium adducts of two cyclic oligomers with different compositions.

detected in the 15–55 min time range were assigned to ammonium and sodium adducts of PLG oligomers (Figure 5). Figure 6 shows +EPI spectra for several selected precursor ions. The assignment was based on the comparison of measured *m/z* values to calculated ones and on analysis of product ion spectra. It must be emphasized that those ions were assigned to cyclic oligomers, not linear ones that are expected to be the most prevalent species.

Formation of cyclic oligomers is obviously possible considering the PLG structure and those species have been prepared and characterized (40). Ions of linear oligomers could also be detected (described later), but intensities of the corresponding MS signals were fairly low. It is conceivable that cyclic PLG oligomers have higher affinity to cations and, therefore, cationization efficiencies are significantly higher for those species. Ionization conditions may also contribute to their in-source formation. Doubly charged ions of PLG oligomers could also be identified by inspecting +ER and +EPI spectra. Independent of the structure of PLG oligomers, their presence is an unusual feature of PLG copolymers. The UV chromatograms (Figure 3) indicated that the high-molecular weight PLG (RT ~56.3 min) significantly changed upon sterilization. Exposure to β-radiation and also to the ambient environment may contribute to the copolymer degradation. LC–MS analysis of paclitaxel/PLG films revealed the presence of PLG oligomers in the non-sterile material as well as material subjected to E-BEAM sterilization (Figure S1 in Supplementary Information).

Very strong MS signals due to PLGA oligomers prevent detection and identification of multiple low-level degradants of ***1*** and, therefore, represent a serious challenge for analytical method development. The complexity of this drug/polymer system is illustrated by the results that we obtained when attempting to apply a recently reported IDA-based strategy for degradant identification (33). This approach, named by the authors as 'N-in-one' strategy, takes advantage of extracted ion chromatograms (XIC) derived from dependent EPI chromatograms. Product ions of the original compound of interest can be used to generate XIC profiles that, in turn, have to be inspected to identify precursor ion corresponding to metabolites or degradants.

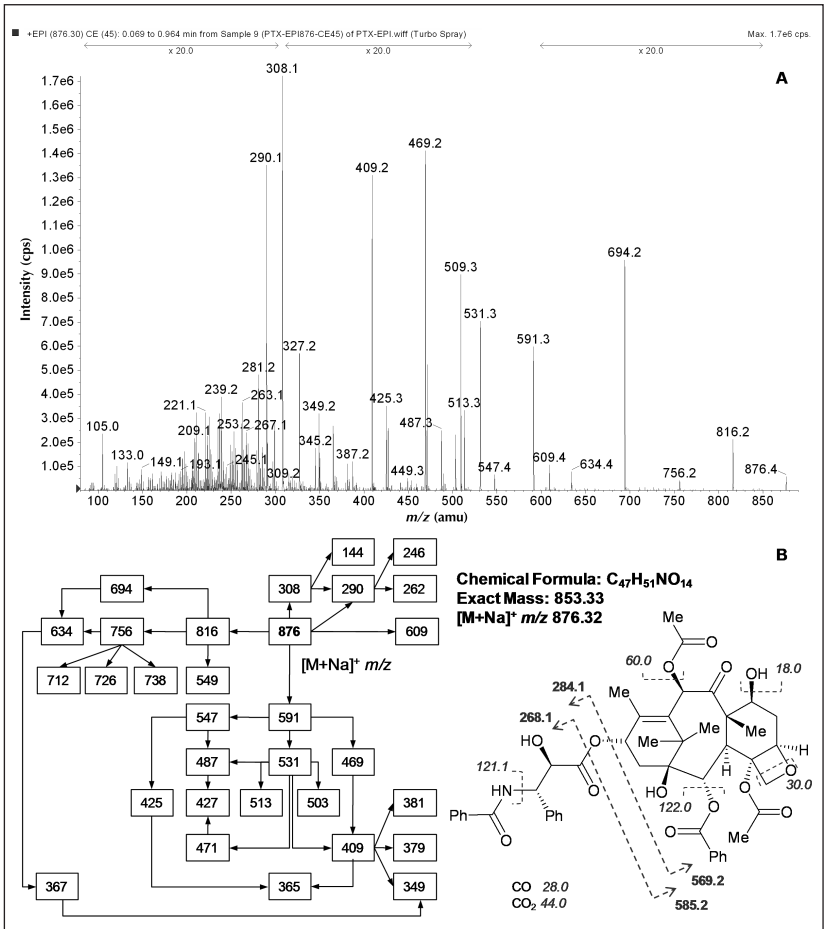

Figure 7. (A) Enhanced product ion (+EPI) spectrum for the m/z 876.3 precursor ion. The spectrum was acquired by using direct infusion of 12 µg/mL solution of ***1*** in acetonitrile–water (1:1 v/v). Notice that all the intensities except for those in the *m/z* ranges 307–309, 530–595, and >820 are multiplied by a factor of 20. (B) Proposed CID mechanism for sodiated species. Dashed lines with arrows show two major fragments with their corresponding masses (bold). For neutral losses outlined by dashed brackets, the masses (italic) are given for the corresponding fragments with a hydrogen atom added. Mass-to-charge ratio values of the M-series ions: 876, 816, 756, 738, 726, 712, 694, 634, 609; T-series ions: 591, 547, 531, 513, 503, 487, 471, 469, 427, 425, 409, 381, 379, 365, 349; S-series: 308, 290, 262, 246, 144.

Figure 7 shows a +EPI spectrum of ***1*** and a proposed mechanism of CID for the $[M+Na]^+$ ion. The mechanism was established by combining the MS–MS data for different collision energies and the results of MS–MS–MS experiments. The fragmentation mechanism was found to be generally similar to that established for $[M+H]^+$ and $[M+NH_4]^+$ ions of ***1*** (10,41–43). The three most intense signals for the fragment ions were characterized by *m/z* of 591.3, 531.3, and 308.1. Three ion series corresponding to the full molecule (M-series), its cyclic core (T-series), and the side chain (S-series) were easily identified. The facile loss of a water molecule from the diterpene core that was observed for protonated ions (*m/z* 569 → 551) could not be detected for the sodium adduct (notice the absence of *m/z* 573 peak in Figure 7). Similar behavior has been reported in the earlier study (36) where FAB mass spectra and CID of alkali metal adducts of ***1*** were investigated.

Another distinct feature of the $[M+Na]^+$ fragmentation was the loss of a 44 u fragment, presumably CO_2. The reaction leads to ions with *m/z* 547 and 487 that have no analogs among protonated non-radical species reported in the literature (41–43). This mode of CID was not mentioned in the FAB MS study of alkali metal adducts. Our MS–MS–MS experiments for ***1*** and ***3*** did not provide evidence for the sequential fragmentation of the side chain ion ($[M+Na]^+$ *m/z* 308) leading to sodiated benzamide (*m/z* 144). In contrast to the previous reports for the protonated species, the latter ion appeared to be formed directly from the *m/z* 308 ion.

The XIC chromatograms corresponding to the three major fragment ions (*m/z* 591.3, 531.3, and 308.1) were generated for the sterilized stent extract (Figure 8). Those profiles revealed only a few degradation products of ***1***. Moreover, numerous false positive signals were observed. Inspection of the +EPI

spectra suggested that strong chromatographic peaks observed within the time window 20–27 min in the *m/z* 531–532 XIC trace were due to PLG oligomers. PLG interferences could not be eliminated, even when a very narrow *m/z* range (531.2–531.4) was used (see Figure S2). Figure 9 presents the +EPI spectra that confirm our assignment of those peaks to sodium adducts of linear PLG oligomers.

The data discussed above were acquired by using just one dependent EPI scan. One possibility to obtain more structural and mechanistic information might be the use of multiple ions as triggers and multiple dependent scans. This, however, would necessarily increase the duty cycle, which was already fairly long (~0.5 s), so that a larger number of species might escape identification. To overcome those difficulties, we adopted an iterative combination approach, which is outlined in Figure 10. Two complementary survey scans were used for building IDA-type LC–MS–MS methods. Those methods were applied to both stent samples and sterilized drug substance, which served as a mechanistic model. Additional mechanistic information was obtained from the LC–MS–MS analysis of the two compounds corresponding to the fragments of ***1***: the diterpene core, ***2***, and the side chain, ***3***. UV and MS chromatograms for ***1–3*** are presented in Figures S3–S5 of the Supplementary Information.

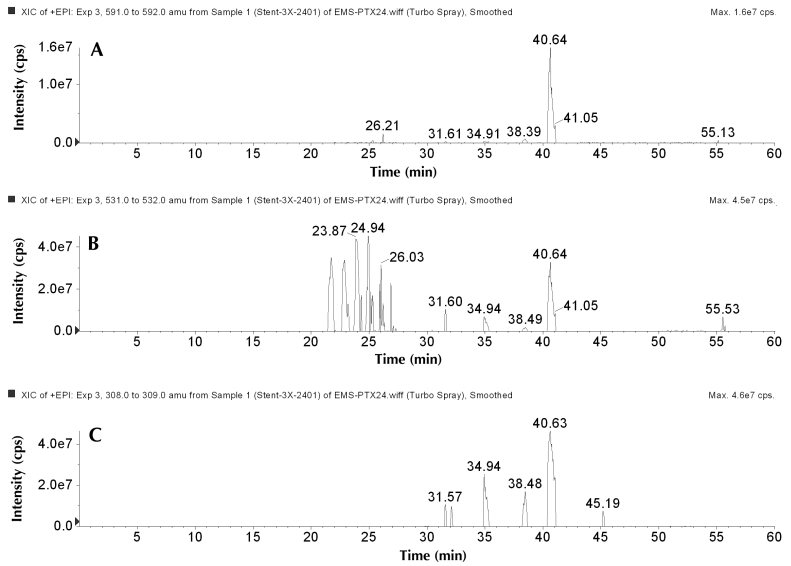

Figure 8. LC–MS–MS analysis of paclitaxel/PLG mixtures from COSTAR Stents sterilized by E-BEAM to a dose of 75 kGy. Extracted ion current chromatograms (XIC of +EPI) for m/z 591–592 (A), 531–532 (B), and 308–309 (C) are shown. Mobile phase: A1/B1.

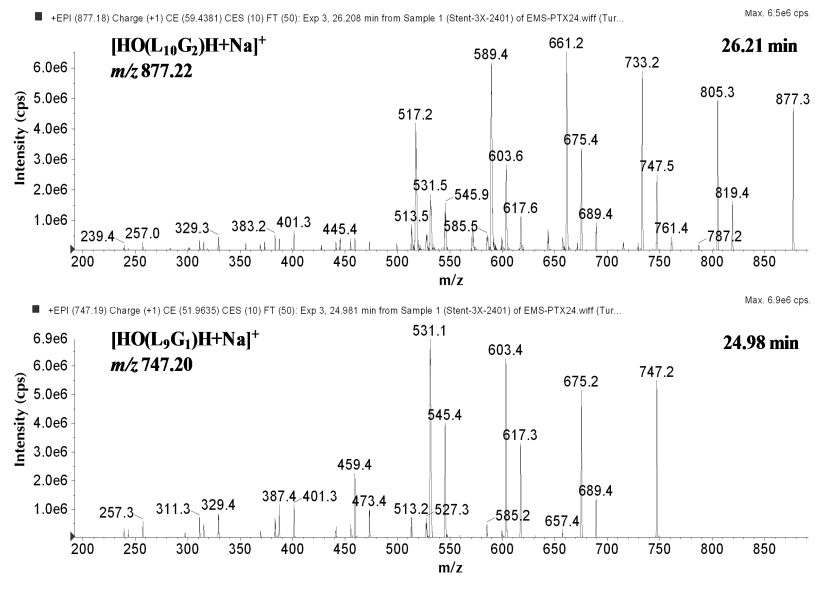

Figure 9. LC–MS–MS analysis of paclitaxel/PLG mixtures from stressed COSTAR Stents sterilized by E-BEAM to a dose of 75 kGy. Enhanced product ion spectra recorded at 26.21 min (top) and 24.98 min (bottom) were attributed to sodiated PLG oligomers. Notice strong signals around m/z 531 ($[OH(L_6G_1)H+Na]^+$ *m/z* 531.13). Mobile phase: A1/B1.

When +EMS-based IDA was applied to the sterilized drug substance and its fragments, the MS data revealed the vast majority of the degradation products. Reconstruction of XIC profiles based on TIC of +EPI chromatograms and selected product ions that were identified by MS–MS analysis of unstressed materials was shown to be an efficient way of data processing (see Figure S6 in Supplementary Information). Analysis of ***3*** also emphasized the importance of the proper selection of the mobile phase. Chromatography of this compound, which is a carboxylic acid, was strongly affected by a secondary equilibrium due to protolytic dissociation. Multiple broad peaks were observed when a non-buffered mobile phase was used (see data for A1/B1 in Figure S5, Supplementary Information).

MS–MS identification of the major degradation products in sterilized materials of ***1–3*** allowed selecting MRM transitions to build another IDA method. The latter method was utilized to identify degradants in drug/PLG mixtures. Figure 11 compares XIC profiles based on ten ion pairs that were used in the +MRM scan for the stent extract and the drug substance. Although the majority of degradants were present in both samples, their relative quantities seemed to differ substantially between the drug substance and the COSTAR Stent. This observation was supported by analysis of the UV chromatograms. For example, a degradant with an RT of 35.1 min (corresponds to an RT of 34.9 min, *m/z* 894.4 in mass chromatograms) accounted for 3.1% of the total area under the curve (2-50 min) for the stent sample and only for 0.2% for the drug substance (radiation dose of 75 kGy). Nonetheless, our approach was proven to provide valuable information on degradation pathways and products formed in drug/polymer mixtures. Further data mining for +EMS-dependent IDA allowed identifying some other degradants whose structure could be elucidated with +EPI data. The MRM list could be further expanded to incorporate ion transitions for those degradation products that escaped detection

with the original method. Moreover, two survey scans (EMS and MRM) could be combined into a single run to build a powerful IDA method. The results of LC–MS–MS studies are summarized in Table I.

Mass spectral identification based on IDA with either +EMS or +MRM as a survey scan and +EPI as a dependent scans was accomplished for 45 degradation products and impurities. Forty-one of those species were detected either in the sterilized drug substance, in drug/PLG mixtures from COSTAR stents or in both. Four degradants could be detected exclusively in baccatin III (*2*) subjected to E-BEAM irradiation. An isomer of *2* (RT 26.05 min) and its dehydrogenated derivative (RT 28.62 min, *m/z* 607.3), albeit being detected in all samples, did not show significant accumulation with the radiation dose. The formation of acid *3* in either drug substance or drug/PLG mixtures was not confirmed by +EPI, but a weak peak with an RT close to 23.2 min, as that in the authentic material, could be observed in the mass chromatograms (XIC of +EMS, *m/z* 308–309) that were obtained with the acidified mobile phase (A2/B2). By using only 10 ion pairs for the +MRM-based acquisition method we could unambiguously identify 28 degradants. Five of those species were detected exclusively in the sterilized stent extract, and three were found exclusively in the E-BEAM treated drug substance. According to HPLC-UV data, 27 peaks with area percent ranging from 0.1% to 3.1% accounted for 13.0% of the total area attributed to the degradants in the stents irradiated to the 75 kGy dose.

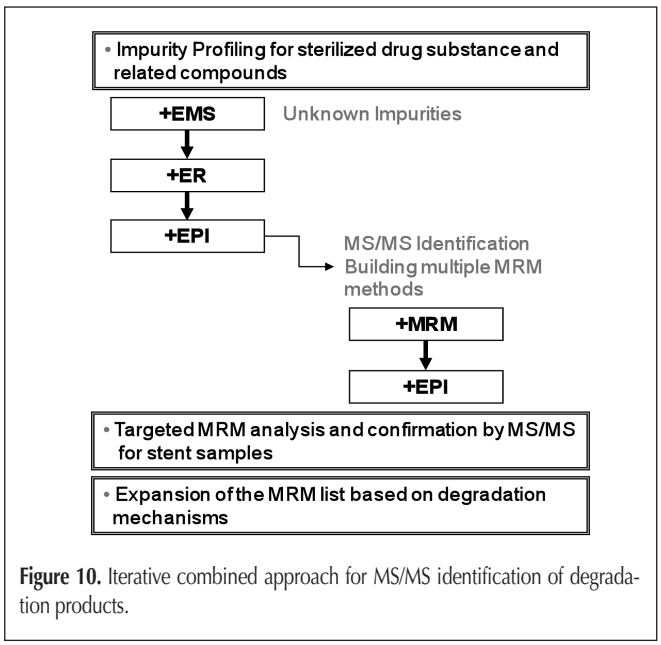

Figure 10. Iterative combined approach for MS/MS identification of degradation products.

By combining the UV and MS data, the most abundant degradants were identified as isomers of *1* and of its derivatives with molecular masses increased by 18, 16, or 14 u. The latter compounds presumably arise through addition of a water molecule, an oxygen atom, or O_2 and the removal of a water molecule. These addition reactions were found to take place in the cyclic diterpene core of the *1* molecule. Oxidative mechanisms of the radiation-induced degradation were also evident from the formation of dehydrogenated compounds ($[M+Na]^+$ *m/z* 874 and 607). Compound *4* (an isomer of *1* with an RT of 31.6 min) was observed as an abundant degradant in both the drug substance and COSTAR Stent fillings sterilized with E-BEAM. For the drug substance, this isomer appeared to be the main degradation product accumulated in a dose-dependent manner. The +EPI spectra (*m/z* 876.3), acquired within the chromatographic peaks corresponding to *1* and *4* (see Figure S7), revealed distinct structural differences. CID of the sodium adduct of *1* resulted in the formation of ions with *m/z* 425, 469, and 547. These ions were practically absent when the sodiated *4* was fragmented. In contrast, the +EPI spectrum of *4* showed strong signals at *m/z* 816, 756, 634, and 471 that were diminished in the mass spectrum of *1*. Another paclitaxel isomer with an RT of 36.4 min appeared to be structurally related to *4* (see Figure S7b). The +MRM scan for *m/z* 876.4/531.3 revealed fairly strong signals covering the entire time range of 31.6–36.4 min. These findings suggested a secondary equilibrium between *4* and the RT 36.4 min isomer that was establishing on a time scale comparable to that for the LC separation. Such a secondary equilibrium may contribute the mass balance problem observed for the HPLC-UV data. An isomer of *1* eluting at 46.35 min (see Table I) could be assigned to 7-epimer by comparing the HPLC-UV and –MS data for the sterilized materials and 13-Taxane HPLC Mix Standard.

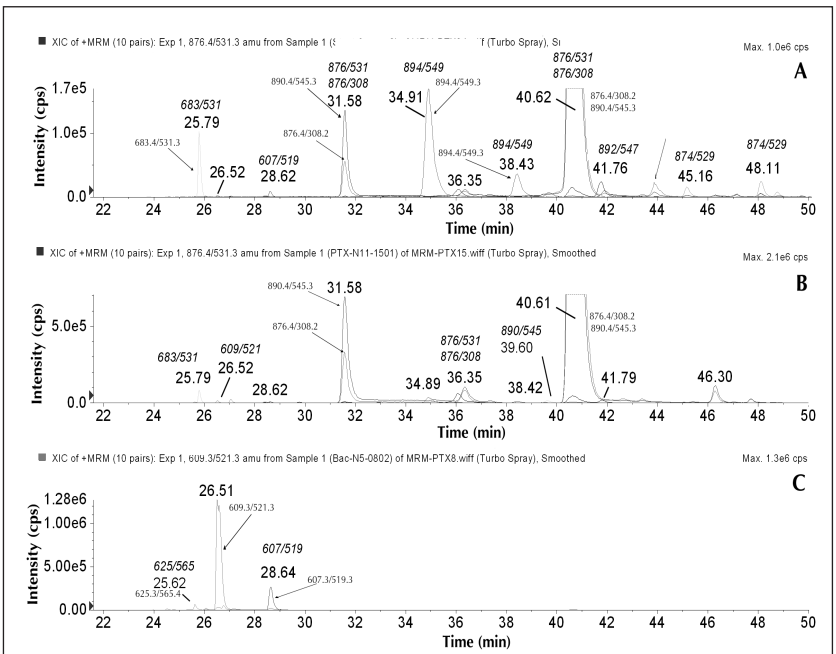

Figure 11. LC–MS–MS analysis of paclitaxel/PLG mixtures from COSTAR Stents (A), paclitaxel drug substance (B), and baccatin III (C). All materials were sterilized by E-BEAM to a dose of 75 kGy. Extracted ion current (XIC of +MRM) chromatograms for the following m/z pairs are shown: 876.4/531.3, 876.4/308.2, 894.4/549.3, 892.4/547.3, 890.4/545.3, 874.4/529.3, 683.4/531.3, 625.3/565.4, 609.3/521.3, and 607.3/519.3. Mobile phase: A1/B1.

Extracted ion chromatograms were generated for potential degradation products of *1* and *2*, namely those with the side chain, acetate or benzoate ester being hydrolyzed, or all combinations

thereof. Except for baccatin III and an *m/z* 567 degradant, which formally corresponds to deacetylbaccatin III, no corresponding ion signals were found. Analysis of the enhanced product ion spectrum of the *m/z* 567 degradant indicated that this compound may be related to baccatin III, but still may contain two acetyl groups (two neutral loss of 60 u). Further studies are needed to clarify its structure and origin. Formation of baccatin III (***2***) in a dose-dependent manner was observed, but the *m/z* 609 signal (RT 26.5 min) corresponding to ***2*** was fairly weak. A complimentary fragment for *m/z* 609 degradants could not be easily detected by MS. Still weak peaks with RT close to 23.2 min could be observed in the mass chromatograms (XIC of +EMS, *m/z* 308–309) when the acidified mobile phase (A2/B2) was used. A distinct peak with the corresponding RT was also observed in the UV chromatograms of the sterilized drug substance.

Only a few degradants (see Table I) were produced through modifications on the side chains. Among those, a derivative of ***2*** (RT 25.8 min, *m/z* 683.4) could be identified by using +ER and +EPI spectra. The latter compound accounted for ~1% of the total area under the curve for the 230 nm chromatogram of COSTAR Stents irradiated to a dose of 75 kGy. The odd *m/z* value for this species was consistent with the loss of the N-containing moiety from the side chain of ***1***. A possible degradation mechanism leading to the formation of two compounds that yield sodium adducts with *m/z* 248 and 683 is presented in Figure 12. The reaction involves oxidative cleavage of the *i*-serine moiety. The *m/z* 683 degradant (***5***) was assigned to an ester of the glyoxalic acid hydrate and ***2***. This assignment was supported by neutral losses of 74 u (glyoxalic acid) and 92 u (glyoxalic acid hydrate) observed in the +EPI spectrum of ***5*** (see Figure S8). The remaining portion of the drug molecule was converted to dibenzimide (***6***), which could be associated with a degradant eluting at

Table IA. Mass Spectral Identification of Degradation Products of 1–3 in E-BEAM Sterilized Samples

ID No.	*m/z*	RT (min)	RRT	MRM* *m/z*	MRM/ EPI†	EMS/ EPI‡	Major Product Ions	Tentative Assignment and Comments§
D1	681.2	21.70	0.536	-	-	P	591, 549, 531, 469, 427, 409, 206	B+3O+2C; A1:B1 only**
3	308.1	23.19	0.571	-	-	A	290, 264, 262, 144	A; Side-chain acid (**3**)
D2	625.2	24.54	0.604	625/565	B	B	607, 565, 547, 519, 475, 443	B+1O
D3	248.1	25.01	0.616	-	-	A, P, S	230, 162, 144	A-2O-2C-4H
D4	627.3	25.20	0.621	-	-	B	567, 549, 505, 445, 427, 401, 375, 197	B+1O+2H
D5	625.3	25.62	0.631	625/565	B, P, S	B, P	607, 595, 565, 547, 537, 443, 383	B+1O
D6	641.2	25.77	0.635	-	-	B	623, 581, 553, 519, 431, 387, 377, 305	B+2O
D7	683.4	25.79	0.635	683/531	P, S	P	623, 609, 591, 531, 469, 409, 349, 263	B+3O+2C+2H
D8	609.2	26.05	0.641	609/521	B, P, S	B, P	549, 521,489, 461, 427, 367, 337	B (isomer of ***2***); No change with E-BEAM
D9	228.3	26.28	0.647	-	-	A, P	210, 184	A-2O-2C-2H; $[M+H]^+$; A2:B2 only
2	609.3	26.51	0.653	609/521	B, P, S	B, P	549, 521, 489, 459, 427, 367, 337, 309	B, Baccatin III (***2***)
D10	625.3	26.56	0.654	625/565	B, P, S	B	607, 565, 547, 521, 503	B+1O; Also at 26.75 min in B
D11	625.3	27.05	0.666	625/565	B, P, S	B, P	607, 565, 549, 537, 533, 519, 504, 427, 397	B+1O; peak overlap in B
D12	641.2	27.76	0.684	-	-	B	623, 581, 553, 519, 431, 387, 377, 305	B+2O
D13	607.3	28.62	0.704	607/519	B, P, S	B, P	547, 519, 487, 457, 425, 365, 337	B-2H; No change with E-BEAM
D14	842.2	28.98	0.714	-	-	P	591, 531, 469, 409, 349, 274	P-2O-2H, side chain; A1:B1 only
D15	593.3	30.50	0.751		-	P	533, 443, 411, 351	B-1O; A1:B1 only
4	876.4	31.59	0.778	876/531 876/308	P, S	P, S	816, 756, 634, 591, 531, 471, 308, 290, 262	P Photodegradant (***4***)
D16	892.4	31.86	0.785	-	-	P	832, 710, 591, 531, 409, 324, 306	P+2O, side chain
D17	892.4	32.96	0.812	892/547	P, S	-	832, 770, 710, 607, 547, 529, 425, 308	P+1O, core; weak in P
D18	842.4	33.27	0.819	-	-	P	591, 531,469, 409, 381, 349, 274	P-2O-2H; side chain; A1:B1 only
D19	894.4	34.91	0.860	894/549	P, S	P, S	772, 712, 609, 549, 531, 487, 427, 308, 290	P+1O+2H, core
D20	892.4	36.07	0.888	892/547	D, S	S	832, 770, 710, 607, 547, 529, 425, 308, 290	P+1O, core
D21	876.4	36.35	0.895	876/531 876/308	P, S	P,	816, 756, 634, 591, 531, 409, 308, 290	P; related to ***4***
D22	908.2	37.44	0.922	-	-	P	623, 607, 547, 519, 425, 397, 308, 290	P+2O, core
D23	832.3	37.40	0.921	-	-	P	744, 650, 590, 547, 425, 308	P-2O-1C, core
D24	832.3	37.85	0.932	-	-	P	650, 590, 547, 487, 425, 308, 290	P-2O-1C, core
D25	894.4	38.38	0.945	894/549	P, S	P, S	772, 712, 609, 549, 487, 427, 308, 290, 197	P+1O+2H, core
D26	856.5	38.60	0.951	-	-	P	674, 591, 531, 409, 288, 270	P-1O-4H, side chain
D27	908.2	39.09	0.963	-	-	P	623, 581, 563, 521, 371, 308, 290	P+2O, core; A1:B1 only
D28	890.4	39.60	0.975	890/545	P	P	830, 605, 563, 545, 517, 423, 308, 290	P+1O-2H, core
D29	894.4	39.71	0.978	894/549	S	-	834, 772, 712, 609, 549, 531, 308	P+1O+2H, core

* Detection by +MRM scans using *m/z* pairs shown, see Figure 8 caption for the exact *m/z* values;
† Identification by +EPI with +MRM as survey scan; S: COSTAR Stents; P: Paclitaxel (**1**) drug substance; B: Baccatin III (**2**); A: *N*-benzoyl-3-phenyl-iso-serine (**3**);
‡ Identification by +EPI with +EMS as survey scan; S: COSTAR Stents; P: Paclitaxel (**1**) drug substance; B: Baccatin III (**2**); A: *N*-benzoyl-3-phenyl-iso-serine (**3**);
§ 'P' corresponds of a mass of 853 u; 'B' - to a mass of 586 u; 'A' - to a mass of 285 u;
** A1:B1 only: Observed only with the A1:B1 mobile phase; A2:B2 only: Observed only with the A2:B2 mobile phase; Side chain: Modification in the side chain; Core: Modification in the diterpene core; No change with E-BEAM: The peak area did not change upon E-BEAM sterilization.

25.0 min. This compound could be detected in both stent extracts and sterilized materials, ***1*** and ***3***. XIC chromatograms for *m/z* 247.5–248.5 showed a distinct peak at 25 min for the sterilized samples. An absorption spectrum recorded at 25.1 min differed substantially from that of ***1*** (see Figure S9 in Supplementary Information). A bathochromic shift seen in the absorption spectrum of the *m/z* 248 degradant is consistent with the proposed structure. Another minor product with an RT of 21.70 min and *m/z* 681 is most likely to be an oxidized form of ***5*** (i.e., an ester of oxalic acid and ***2***).

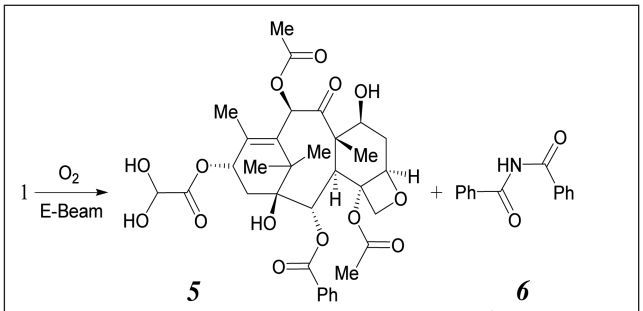

Figure 12. Proposed mechanism of oxidative cleavage of ***1*** under E-BEAM sterilization conditions.

As mentioned above, a mass–balance problem was uncovered when initial HPLC-UV data for sterilized stents were analyzed. The issue could not be resolved despite significant efforts aimed at optimization of the HPLC method. The results obtained in this study indicated that multiple factors likely contributed to the mass balance problem. The fact that so many low-level degradation products were formed upon sterilization made clear that accurate quantitation might be difficult. In addition, we found that PLG oligomers were co-eluting with degradation products of ***1***. Although PLG polymers exhibit very weak molar absorption at 230 nm, their absorption spectra do extend to that region. Consequently, these compounds may affect the base line of UV chromatograms and may interfere with quantitation of ***1*** and its derivatives. More importantly, the LC–MS data indicated that a secondary equilibrium might exist for ***4***, which is an isomer of ***1*** and one of the most abundant degradants. Other products, such as dehydrogenated species *m/z* 874.4, might be also involved in equilibrium reactions taking place in the course of LC separation. If the time scale for such secondary equlibria and the primary one associated with the chromatographic separation are comparable, a significant portion of the signal may be lost because of peak broadening and tailing. In the *m/z* 876–877 chromatograms (see Figure 11 and Figure S10 in Supplementary Information), we observed a signal bridging the gap

Table IB. Mass Spectral Identification of Degradation Products of 1–3 in E-BEAM Sterilized Samples

ID No.	*m/z*	RT (min)	RRT	MRM* *m/z*	MRM/ EPI†	EMS/ EPI‡	Major Product Ions	Tentative Assignment and Comments§
1	876.4	40.61	1.000	876/531 876/308	P, S	P, S	816, 694, 591, 531, 469, 409, 308, 290	P, Paclitaxel: ***1***
D30	892.4	41.76	1.028	892/547	P, S	P	832, 770, 710, 607, 547, 531, 529, 425, 308	P+1O, core
D31	876.4	41.90	1.032	876/531 876/308	S	-	816, 694, 591, 547, 531, 308	P
D32	876.4	42.58	1.049	876/531 876/308	-	P	816, 788, 666, 606, 591, 531, 409, 308	P
D33	876.4	43.87	1.080	876/531 876/308	S	P	816, 751, 694, 591, 531, 308, 290	P
D34	870.4	44.50	1.096	-	-	P	688, 591, 531, 409, 302, 284	P-6H, side chain A1:B1 only
D35	890.4	44.80	1.103	890/545	P	-	830, 768, 708, 605, 545, 308	P+1O-2H, core
D36	874.4	45.16	1.112	874/529	P, S	P, S	814, 754, 692, 591, 589, 529, 469,308	P-2H, core
D37	876.3	46.35	1.141	876/531 876/308	P, S	P	816, 694, 591, 531, 409, 308, 290	P
D38	874.4	46.67	1.149	874/529	P, S	P	814, 754, 692, 589, 529, 407, 308, 290	P-2H, core
D39	874.4	47.04	1.158	874/529	P, S	P	814, 754, 632, 547, 529, 308, 262	P-2H, core
D40	876.4	47.12	1.160	876/531 876/308	S	-	816, 694, 591, 531, 308	P
D41	876.4	47.70	1.175	876/531 876/308	P	P	816, 591, 549, 531, 409, 308, 290	P
D42	874.4	48.11	1.185	874/529	P, S	-	814, 754, 692, 589, 529, 407, 308	P-2H, core
D43	874.4	48.76	1.201	874/529	S	-	814, 754, 692, 589, 529, 308	P-2H, core

* Detection by +MRM scans using *m/z* pairs shown, see Figure 8 caption for the exact *m/z* values;
† Identification by +EPI with +MRM as survey scan; S: COSTAR Stents; P: Paclitaxel (**1**) drug substance; B: Baccatin III (**2**); A: N-benzoyl-3-phenyl-iso-serine (**3**);
‡ Identification by +EPI with +EMS as survey scan; S: COSTAR Stents; P: Paclitaxel (**1**) drug substance; B: Baccatin III (**2**); A: N-benzoyl-3-phenyl-iso-serine (**3**);
§ 'P' corresponds of a mass of 853 u; 'B' - to a mass of 586 u; 'A' - to a mass of 285 u;
** A1:B1 only: Observed only with the A1:B1 mobile phase; A2:B2 only: Observed only with the A2:B2 mobile phase; Side chain: Modification in the side chain; Core: Modification in the diterpene core; No change with E-BEAM: The peak area did not change upon E-BEAM sterilization.

between the peaks of *4* and its analog with the area under the curve comparable to that of the main peak. Such a signal would not be resolved from the base line in UV chromatograms and would therefore be lost.

An additional complication with the quantitation of paclitaxel degradants arise from the fact that some of them are acids that may again be involved in slow secondary equilibria if non-buffered mobile phases are used. On the other hand, some degradants are expected to be fairly unstable in concentrated buffers because many possible secondary reactions are expected to exhibit both specific and general acid/base catalysis. Five compounds among the degradation products identified (Table I) could only be detected when the non-buffered mobile phase (A1/B1) was used. These factors make selection and optimization of the mobile phase and other separation conditions extremely difficult. Formation of volatile compounds may also be responsible, at least partially, for non-accounted drug loss upon E-BEAM sterilization. A recent GC–MS study revealed the presence of such compounds in sterilized samples (44).

Conclusion

Mixtures of paclitaxel (*1*) with PLG that were sterilized by E-BEAM presented significant challenges for analytical method development. HPLC-UV data revealed numerous degradation products of *1* that were formed in a β-radiation dose-dependent manner to give a plethora of low-level degradants. Mass balance could not be achieved using UV-detection alone, despite strong efforts to optimize HPLC-UV methods and to improve their performance. Standard LC–MS methods utilizing full mass scans faced additional challenges due to multiple interferences from PLG oligomers. Those oligomeric species appeared to be present in PLG raw materials and also were likely formed upon β-irradiation that strongly affected the high-molecular weight copolymer. To identify degradants in such complex mixtures, we adopted an iterative approach based on LC–MS–MS techniques with information-dependent acquisition (IDA). This type of analysis, when applied to sterilized drug substance and the two compounds representing its side chain (*3*) and the diterpene core (*2*), allowed identifying major pathways of paclitaxel degradation under E-BEAM sterilization conditions used. Isomerization, together with oxidative and hydrolytic processes, appeared to account for the vast majority of the degradants. These results enabled development of selective MRM-based IDA-methods for identification of low-level degradation products in drug/PLG mixtures. Twenty-eight species could be identified by using such a method with 10 MRM pairs. Only five of them could be revealed by applying an IDA method with +EMS as a survey scan. Although E-BEAM degradation mechanisms were found to be similar for sterilized stents and the drug substance, significant discrepancies were also observed. This finding emphasized the importance of the iterative approach with IDA methods utilizing different (or multiple) survey scans, including MRM scans, with the ion pair list being expanded in accordance with an evolving understanding of degradation reaction mechanisms. The results also indicated that multiple factors might contribute to the mass-balance problem encountered in HPLC-UV analysis. The fact that many degradation products were labile (isomerize, decompose, etc.) even under very mild separation conditions used indicated that this mass-balance problem could not be resolved without systematic investigation of paclitaxel reaction mechanisms and kinetics.

Supplementary Information Available

Figures S1–S10 with chromatograms and mass spectra are available upon request and can be found in the digital version of the manuscript.

Acknowledgments

The authors want to thank Ronald Dadino (Cordis Corp.) for continuous support, Thomas Harper and Frederick Halperin (J&J Sterile Process Technology) and E-BEAM Services, Inc. for technical assistance with the E-BEAM sterilization. Many thanks are due to Bethany Harris for helping with the manuscript preparation.

References

1. N.I. Marupudi, J.E. Han, K.W. Li, V.M. Renard, B.M. Tyler, and H. Brem. Paclitaxel: a review of adverse toxicities and novel delivery strategies. *Expert Opin. Drug Saf.* **6(5):** 609–621 (2007) and reference therein.
2. J.F. Diaz, J.M. Andreu, and J. Jimenez-Barbero, The interaction of microtubules with stabilizers characterized at biochemical and structural levels. *Top. Curr. Chem.* **286:** 121–149 (2009) and reference therein.
3. *Handbook of Drug-Eluting Stents*; P.W. Serruys and A.H. Gershlick, Eds. Taylor & Francis, London, 2005, p. 369.
4. A. Rastogi and S. Stavchansky. Drug eluting stents and beyond. *Curr. Pharm. Des.* **14(21):** 2111–2120 (2008).
5. S. Chatterjee and A. Pandey. Drug eluting stents: friend or foe? A review of cellular mechanisms behind the effects of paclitaxel and sirolimus eluting stents. *Curr. Drug Metab.* **9:** 554–566 (2008).
6. J. Aragon and F. Litvack. In *Handbook of Drug-Eluting Stents*; P.W. Serruys, and A.H. Gershlick, Eds. Taylor & Francis, London, 2005, pp. 227–232.
7. M.W. Krucoff, D.J. Kereiakes, J.L. Petersen, R. Mehran, V. Hasselblad, A.J. Lansky, P.J. Fitzgerald, J. Garg, M.A. Turco, C.A. Simonton, S. Verheye, C.L. Dubois, R. Gammon, W.B. Batchelor, C.D. O'Shaughnessy, J.B. Hermiller, J. Schofer, M. Buchbinder, and W. Wijns. A novel bioresorbable polymer paclitaxel-eluting stent for the treatment of single and multivessel coronary disease. *J. Am. Coll. Cardiol.* **51(16):** 1543–1552 (2008).
8. T.Y. Wang, V. Hasselblad, J.L. Peterson, W. Wijns, A. Parhizgar, D.J. Kereiakes, and M.W. Krucoff. The cobalt chromium stent with antiproliferative for restenosis II (COSTAR II) trial study design: advancing the active-control evaluation of second-generation drug-eluting stents. *Am. Heart J.* **153(5)**: 743–748 (2007).
9. D.G.I. Kingston, P.G. Jagtap, H. Yuan and L. Samala. The chemistry of taxol and related taxoids. *Prog. Chem. Org. Natural Prod.* **84**: 53–225 (2002) and reference therein.
10. K.J. Volk, S.E. Hill, E.H. Kerns, and M.S. Lee. Profiling degradants of paclitaxel using liquid chromatography-mass spectrometry and liquid chromatography-tandem mass spectrometry substructural techniques. *J. Chromatogr. B*. **696(1):** 99–115 (1997).
11. I. Ringel and S.B. Horwitz. Taxol is converted to 7-epitaxol, a biologically active isomer, in cell culture medium. *J. Pharmacol. Exp. Ther.* **242(2)**: 692–698 (1987).
12. S.H. Pyo, J.S. Cho, H.J. Choi and B.H. Han. Evaluation of paclitaxel rearrangement involving opening of the oxetane ring and migration of acetyl and benzoyl groups. *J. Pharm. Biomed. Anal.* **43:** 1141–1145 (2007).
13. G. J. MacEachern-Keith, L. J. Wagner Butterfield, and M. J. Incorvia Mattina. Paclitaxel Stability in Solution. *Anal. Chem.* **69(1):** 72–77 (1997).
14. J. Leslie, J.M. Kujawa, N. Eddington, M. Egorin, and J. Eiseman. Stability problems with taxol in mouse plasma during analysis by liquid chromatography. *J. Pharm. Biomed. Analy.* **11(11–12):** 1349–1352 (1993).
15. R.E. Richard, M. Schwarz, S. Ranade, A.K. Chan, K. Matyjaszewski, and

B. Sumerlin. Evaluation of arylate-based block copolymers prepared by atom transfer radical polymerization as matrices for paclitaxel delivery from coronary stents. *Biomacromol.* **6(6):** 3410–3418 (2005).
16. C. Dilcher, R. Chan, D. Hellinga, R. Seabron, R. Pakala, P.K. Kuchulakanti, R. Richard, K. Chan, S. Zhong, J.J. Barry, and R. Waksman. Effect of ionizing radiation on the stability and performance of the TAXUS Express2 paclitaxel-eluting stent. *Cardiovasc. Rad. Med.* **5(3):** 136–141 (2004).
17. E. Ruel-Gariepy, M. Shive, A. Bichara, M. Berrada, D. Le Garrec, A. Chenite, J.C. Leroux. A thermosensitive chitosan-based hydrogel for the local delivery of paclitaxel. *Eur. J. Pharm. Biopharm.* **57(1):** 53–563 (2004).
18. (a) S.H. Chen, C.M. Combs, S.E. Hill, V. Farina, and T.W. Doyle. The photochemistry of taxol: synthesis of a novel pentacyclic taxol isomer. *Tetrahedron Lett.* **33(50)**: 7679–7680 (1992). (b) S.H. Chen, V. Farina, S. Huang, Q. Gao, J. Golik, and T.W. Doyle. Studies on the photochemistry of taxol. *Tetrahedron* **50(29):** 8633–8650 (1994).
19. P.J. Jansen, W.K. Smith, and S.W. Baertschi, Stress testing: analytical considerations. In *Pharmaceutical Stress Testing (Drugs and the Pharmaceutical Sciences).* S.W. Baertschi, Ed. Taylor & Francis, New York, 2006, pp.141–172.
20. J.W. Hager. Q TRAP mass spectrometer technology for proteomics applications. *Drug Discovery Today: Targets* **3(Supplement 1):** S31–S36 (2004).
21. R. King and C. Fernandez-Metzler. The use of Qtrap technology in drug metabolism. *Curr. Drug Metab.* **7(5):** 541–545 (2006).
22. J.W. Hager and J.C.Y. Le Blanc. High-performance liquid chromatography-tandem mass spectrometry with a new quadrupole/linear ion trap instrument. *J. Chromatogr. A.* **1020(1):** 3–9 (2003).
23. G. Hopfgartner, C. Husser, and M. Zell. Rapid screening and characterization of drug metabolites using a new quadrupole-linear ion trap mass spectrometer. *J. Mass Spectrom.* **38(2)**: 138–150 (2003).
24. G. L. Herrin, H.H. McCurdy, and W.H Wall. Investigation of an LC-MS-MS (QTrap) method for the rapid screening and identification of drugs in postmortem toxicology whole blood samples. *J. Anal. Toxicol.* **29(7):** 599–606 (2005).
25. C.A. Mueller, W. Weinmann, S. Dresen, A. Schreiber, and M. Gergov. Development of a multi-target screening analysis for 301 drugs using a QTrap liquid chromatography/tandem mass spectrometry system and automated library searching. *Rapid Commun. Mass Spectrom.* **19(10):** 1332–1338 (2005).
26. B. Tan, H.B. Bradshaw, N. Rimmerman, H. Srinivasan, Y.W. Yu, J.F. Krey, M.F. Monn, J.S.C. Chen, S.S.J. Hu, S.R. Pickens, and J.M. Walker. Targeted lipidomics: discovery of new fatty acyl amides. *AAPS J.* **8(3):** E461–E465 (2006).
27. F.L. Sauvage, F. Saint-Marcoux, B. Duretz, D. Deporte, G. Lachatre, and P. Marquet. Screening of drugs and toxic compounds with liquid chromatography-linear ion trap tandem mass spectrometry. *Clin. Chem.* **52(9):** 1735–1742 (2006).
28. L. Politi, L. Morini, and A. Polettini. A direct screening procedure for diuretics in human urine by liquid chromatography-tandem mass spectrometry with information dependent acquisition. *Clin. Chim. Acta* **386(1-2):** 46–52 (2007).
29. M. Yao, L. Ma, W.G. Humphreys, and M. Zhu. Rapid screening and characterization of drug metabolites using a multiple ion monitoring-dependent MS/MS acquisition method on a hybrid triple quadrupole-linear ion trap mass spectrometer. *J. Mass Spectrom.* **43(10):** 1364–1375 (2008).
30. M.J.M. Bueno, A. Agueera, M.D. Hernando, M.J. Gomez, and A.R. Fernandez-Alba. Evaluation of various liquid chromatography-quadrupole-linear ion trap-mass spectrometry operation modes applied to the analysis of organic pollutants in wastewaters. *J. Chromatogr. A.* **1216(32):** 5995–6002 (2009).
31. A. Jelic, M. Petrovic, and D. Barcelo. Multi-residue method for trace level determination of pharmaceuticals in solid samples using pressurized liquid extraction followed by liquid chromatography/quadrupole-linear ion trap mass spectrometry. *Talanta* **80(1):** 363–371 (2009).
32. K. Scholz, W. Dekant, W. Voelkel, and A. Paehler. Rapid detection and identification of N-acetyl-L-cysteine thioethers using constant neutral loss and theoretical multiple reaction monitoring combined with enhanced product-ion scans on a linear ion trap mass spectrometer. *J. Am. Soc. Mass Spectrom.* **16(12):** 1976–1984 (2005).
33. A.C. Li, M.A. Gohdes, and W.Z. Shou. 'N-in-one' strategy for metabolite identification using a liquid chromatography/hybrid triple quadrupole linear ion trap instrument using multiple dependent product ion scans triggered with full mass scan. *Rapid Commun. Mass Spectrom.* **21(8):** 1421–1430 (2007).
34. S.M.R. Stanley, W.K. Wee, B.H. Lim, and H.C. Foo. Direct-injection screening for acidic drugs in plasma and neutral drugs in equine urine by differential-gradient LC-LC coupled MS/MS. *J. Chromatogr. B.* **848(2):** 292-302 (2007).
35. S.A. Lorenz, P.M. Bigwarfe, Jr., S.V. Balasubramanian, G.J. Fetterly, R.M. Straubinger, and T.D. Wood. Noncovalent dimerization of paclitaxel in solution: evidence from electrospray ionization mass spectrometry. *J. Pharm. Sci.* **91(9)**: 2057–2066 (2002).
36. K.P. Madhusudanan. Alkali metal cationization and its effect on the collision-induced decomposition of taxol. *J. Mass Spectrom.* **30(5)**: 703-707 (1995).
37. J.S.C. Loo, C.P. Ooi, and F.Y.C. Boey. Degradation of poly(lactide-co-glycolide) (PLGA) and poly(l-lactide) (PLLA) by electron beam radiation. *Biomaterials* **26(12)**: 1359–1367 (2005).
38. J.A. Bushell, M. Claybourn, H.E. Williams, and D.M. Murphy. An EPR and ENDOR study of gamma- and beta-radiation sterilization in poly(lactide-co-glycolide) polymers and microspheres. *J. Control. Release* **110(1)**: 49–57 (2005).
39. N.K. Chia, S.S. Venkatraman, F.Y.C. Boey, S. Cadart, and J.S.C Loo. Controlled degradation of multilayered poly(lactide-co-glycolide) films using electron beam irradiation. *J. Biomed. Mater. Res. A* **84(4)**: 980–987 (2008).
40. I. Osaka, M. Watanabe, M. Takama, M. Murakami, and R. Arakawa. Characterization of linear and cyclic polylactic acids and their solvolysis products by electrospray ionization mass spectrometry. *J. Mass Spectrom.* **41(10):** 1369–1377 (2006).
41. T.D. McClure, K.H. Schram, and M.L. Reimer. The mass spectrometry of taxol. *J. Am. Soc. Mass Spectrom.* **3(6):** 672–679 (1992).
42. L.M. Cousins and B.A. Thomson. MS3 using the collision cell of a tandem mass spectrometer system. *Rapid Commun. Mass Spectrom.* **16(11):** 1023–1034 (2002).
43. Y. Konishi, T. Kiyota, C. Draghici, J.M. Gao, F. Yeboah, S. Acoca, S. Jarussophon, and E. Purisima. Molecular formula analysis by an MS/MS/MS technique to expedite dereplication of natural products. *Anal. Chem.* **79(3):** 1187–97 (2007).
44. G. Vas, L. Alquier, C.A. Maryanoff, J. Cohen, and G. Reed. Investigation of mass-balance issue in E-BEAM sterilized paclitaxel eluting coronary stents by SPME/GC-MS. *J. Pharm. Biomed. Analysis* **48(3):** 568–572 (2008).

Manuscript received July 9, 2010;
revision received February 12, 2011.